

# Development of a Direct-Measurement Thin-Film Heat Flux Array

Jerrod A. Ewing

Thesis submitted to the faculty of the  
Virginia Polytechnic Institute and State University  
in partial fulfillment of the requirements for the degree of

Masters of Science  
in  
Mechanical Engineering

Dr. Thomas Diller, Co-Chair  
Dr. Pavlos Vlachos, Co-Chair  
Dr. Scott Huxtable

December 11, 2006  
Blacksburg, Virginia

Keywords: Heat Flux Measurement, Thin Film Heat Flux Gage, Heat Flux

Copyright 2006, Jerrod A. Ewing

# **Development of a Direct-Measurement Thin-Film Heat Flux Array**

Jerrod A. Ewing

Virginia Polytechnic Institute and State University, 2006

Advisors: Dr. Thomas E. Diller and Dr. Pavlos P. Vlachos

## **Thesis Abstract**

A new thin film heat flux array (HFA) was designed and constructed using a series of nickel/copper thermocouples deposited onto a thin Kapton® polyimide film. The HFA is capable of withstanding temperatures up to 300 °C and produces signals of 42  $\mu\text{V}/(\text{W}/\text{cm}^2)$ . As a result of its thin film construction, the HFA has a first order time constant of 32 ms. Calibrations were completed to determine the gage's output as well as its time response. In order to measure the signal from the HFA amplifiers were designed to increase the magnitude of the voltage output. An example case is given where the HFA is used in an experiment to correlate time-resolved heat flux and velocities.

## Acknowledgments

I would like to thank all of the members of my committee for their help and guidance throughout the duration of this project. Dr. Diller was the driving force behind all of the heat flux work. I want to thank him for giving me the opportunity to contribute first as an undergraduate and then during my Masters work and for his calming effect and sound advice during all stages of this project. Dr. Vlachos' guidance has been appreciated, and I admire his energy and drive which will serve as an example for me as I begin my professional career. Without Dr. Huxtable, this project would not have been possible. He was my contact in the MicrON group, and always was a good person to turn to when discussing my depositions.

I would also like to thank the various people who helped in the construction of the Heat Flux Array. These include Ali Hajjiah and Bill Houck, whose guidance in the use of the e-beam was greatly appreciated. Dr. Kathleen Meehan provided support and suggestions whenever I had problems arise in my processing, both with the e-beam and soldering. Dan Huff in the CPES packaging lab was always able to laser drill Kapton® for me, and helped me develop the fluxless soldering process. Dr. Wicks' assistance in the design of the amplifiers and development of the instrumentation was greatly appreciated. He was always available when I needed to discuss a problem I was having with a measurement in the lab.

Thanks to my friends and everyone in the lab. I feel blessed to have such a good group of co-workers who've been able to help in my research, classes, and in life. Special thanks to Andrew Gifford and Dave Hubble who I've worked closely with on a number of different projects. I'd also like to recognize Patrick Leung who I am lucky to have known and counted as a friend. He touched many of us and will be missed by everyone who knew him.

Finally, thanks to my family, both current and future. They were always there to support me and give me encouragement when I needed it. Adie cooked many meals for me and had to deal with me getting stressed out in the final couple of weeks. I wouldn't want to think about what graduate school would have been like without your love and care.

# Table of Contents

Thesis Abstract.....	ii
Acknowledgments.....	iii
Table of Contents.....	iv
List of Figures and Tables.....	v
Attributions.....	vi
Preface.....	vii
Development of a Direct-Measurement Thin-Film Heat Flux Array.....	1
Abstract.....	1
Introduction.....	1
Experimental Facilities and Equipment.....	3
Thin Film Deposition.....	4
Instrumentation.....	4
Heat Flux Calibration.....	5
DPIV Equipment.....	6
Design of the Heat Flux Array.....	7
Calibration.....	9
Test Case.....	16
Conclusions.....	17
References.....	17
Appendix A: Construction of the Heat Flux Array.....	19
Appendix B: Instrumentation.....	23
Appendix C: Uncertainty Estimation.....	27
Conduction Calibration Uncertainty.....	27
Convection Calibration Uncertainty.....	28
Seebeck Coefficient Uncertainty.....	28
Time Response Uncertainty.....	29
Appendix D: Additional Experimental Results.....	31

## List of Figures and Tables

Figure 1.1. Semi-infinite geometry, as applied to thin film gages.....	2
Figure 1.2. Diagram of the direct measurement of heat flux.....	3
Figure 1.3. Diagram of the capacitor built between the HFA and a metal plate.....	5
Figure 1.4. Diagram of the Convection Calibration Facility at Virginia Tech.....	6
Figure 1.5. Thermocouple equivalent circuit of the HFA.....	7
Figure 1.6. Pictures of the two junction configurations for the HFA.....	8
Figure 1.7. Plot of the output from a conduction test.....	10
Figure 1.8. Summary of the resulting sensitivities from the transient conduction test....	11
Figure 1.9. Results curve from the convection calibration facility.....	12
Figure 1.10. Diagram of the HFA used in the Seebeck experiments.....	13
Figure 1.11. Results from the Seebeck coefficient experiment.....	13
Figure 1.12. Response of the HFA to a step input.....	14
Figure 1.13. Zoomed view of the response of the HFA to a step input.....	15
Figure 1.14. Heat flux and velocity results for flow stagnating on a flat plate.....	16
Figure A.1. The e-beam facility.....	19
Figure A.2. The holder that supports the heat sink and substrate in the e-beam.....	20
Figure A.3. Photograph of the crucibles used in e-beam evaporation.....	21
Figure A.4. Diagram of the stack that is inserted into the hot press.....	22
Figure B.1. Picture of a populated PCB.....	23
Figure B.2. Circuit diagram for a single channel of the PCB.....	23
Figure B.3. Diagram of the DAQ connection for use with the measurement system.....	25
Figure B.4. Diagram of an aliased signal.....	26
Figure D.1. Additional conduction calibration results.....	32
Table 1.1. Table of the rise and fall times for five runs of the time response test.....	15
Table C.1. Uncertainty budget for the conduction calibration.....	27
Table C.2. Uncertainty budget for the convection calibration.....	28
Table C.3. Uncertainty budget for the Seebeck coefficient calibration.....	29
Table C.4. Uncertainty budget for the time response calibration.....	30

## **Attributions**

The paper that is the basis for this thesis is co-authored by Andrew Gifford, Dr. Pavlos Vlachos, Dr. Alfred Wicks, and Dr. Thomas Diller. Andrew refined the convection calibration and collected the data used in the discussion of said calibration. He also is making use of the Heat Flux Array in his own experiment, and the example application is the results from his initial test run. Dr. Wicks acted as an advisor for all of the instrumentation portions of the paper, and was instrumental in discovering and solving the capacitance problems that were an issue in the early development of the gage. Dr. Vlachos and Dr. Diller were advisors on the project, and they provided assistance and oversight for all of the work that was completed in this thesis.

# **Development of a Direct-Measurement Thin-Film Heat Flux Array**

## **Preface**

Thin film heat flux arrays (HFAs) are devices designed to make multiple measurements and create a map of the heat flux over a surface. Traditionally, turbomachinery research motivated the development of thin-film arrays. However, thin film arrays can be applied to any area of heat transfer research including biomedical and industrial control processes. The development of the heat flux array was completed under a grant from the National Science Foundation for use in an experiment correlating heat flux and turbulent structures.

This thesis consists of two sections. The first is a journal paper that will be submitted to a heat transfer journal. The paper discusses the design principles behind the heat flux array and reports the results from a series of calibrations. The second section is the appendices which offer documentation supporting the journal paper. Appendix A provides detailed information on the construction of the HFA. Procedural information is included, as well as facility specific details and problems faced while building the HFA. Appendix B gives an outline of the instrumentation that was developed for use with the HFA. General electronic theory and design philosophy give enough background so that the printed circuit boards can be reproduced and used in conjunction with the test equipment in the Complex Thermal Fluids Systems Laboratory to make measurements with the HFA. Appendix C contains the uncertainty calculations for each of the calibrations. Appendix D has additional calibrations that were completed and did not get included into the main body of the thesis.

# Development of a Direct-Measurement Thin-Film Heat Flux Array

Jerrod Ewing, Andrew Gifford, Dr. Pavlos Vlachos, Dr. Alfred Wicks, Dr. Thomas Diller  
Mechanical Engineering Department  
Virginia Polytechnic Institute and State University  
Blacksburg, VA 24061

## Abstract

A new thin film heat flux array (HFA) was designed and constructed using a series of nickel/copper thermocouples deposited onto a thin Kapton® polyimide film. The HFA is capable of withstanding temperatures up to 300°C and produces signals of 40  $\mu\text{V}/(\text{W}/\text{cm}^2)$ . As a result of its thin film construction, the HFA is able to resolve heat flux signals as fast as 32 ms. Calibrations were completed to determine the gage's output as well as its time response. In order to measure the signal from the HFA a bank of amplifiers were designed and built. The design methodology, construction techniques, calibrations, and a test case are all discussed.

## Introduction

Characterization of heat flux is important in a variety of applications where it is desired to effectively transfer thermal energy. Examples include the design of gas turbine blades, industrial process management, and biological systems research.

Thin-film heat flux gages are useful measurement tools because they have a frequency response that is higher than traditional designs such as the Schmidt-Boelter gage [1], and are easier to produce in an array form due to the thin-film techniques used in their construction. The array form allows for the characterization of heat flux over a surface, as opposed to a single point measurement. This capability is important when investigating the effects of non-uniform boundary conditions on heat transfer, such as turbulence, jets, transition, and shock interactions.

Two different types of thin-film heat flux arrays currently exist. One array, developed at Oxford by Schultz and Jones [2], utilizes a semi-infinite transient conduction model to convert surface temperature measurements to heat flux. There are several methods for performing this conversion, either electronically or numerically [3, 4]. The surface temperature measurements are usually made with thin film resistance temperature devices (RTDs), as shown in Figure 1.1. RTDs are thin metal films that change resistance linearly with temperature. One advantage of the semi-infinite gage is that it is capable of extremely high frequency measurements ( $> 200$  kHz). However, the gage can only be

used to capture short time events because the 1-D semi-infinite conduction assumption imposes a time limit, typically of a few seconds. Early models of the semi-infinite heat flux sensor employed machinable glass (MACOR) which has a low thermal conductivity. This minimized 2-D conduction effects in the semi-infinite medium and maximized the amount of time before the heat flux began to cause changes in the semi-infinite temperature.

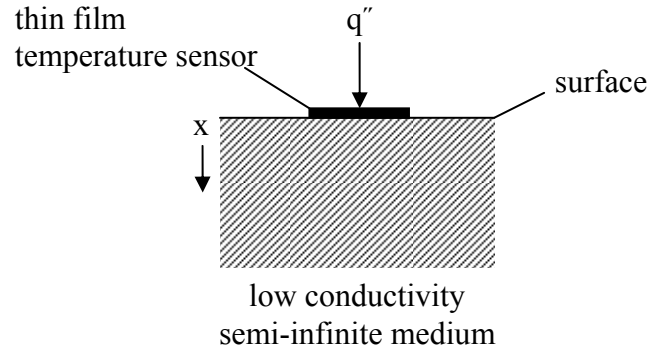


**Figure 1.1.** Semi-infinite geometry, as applied to thin film gages.

Anthony *et al.* [5, 6] constructed their test model so that the entire object, including the substrate that the RTDs were built on, could be modeled as a semi-infinite material. The substrate the sensors were made on was a polyimide (Kapton®), which is commonly used in thin-film applications. The sensors were then mounted onto Perspex that has nearly the same thermal properties as the Kapton® substrate. This enabled multiple layers to be used with a simplified analytical model converting the surface temperature into heat flux.

Piccini *et al.* [7] used a polyimide sheet of gages mounted onto a test model made of metal with a thermocouple pressed into it to measure the metal's temperature. The temperature read by the thermocouple is assumed to be the temperature at the underside of the polyimide since the metal has a high thermal conductivity. With RTDs reading the top surface temperature, the temperature difference ( $\Delta T$ ) across the polyimide provides a direct measurement of the heat flux ( $q''$ ) from a 1-D Fourier's Law analysis

$$q'' = \frac{k}{\delta} \Delta T \quad (1.1)$$

where  $k$  and  $\delta$  are the thermal conductivity and thickness of the resistance layer respectively. The quantity of  $k/\delta$  must be calibrated to measure the heat flux. The calibration done by Piccini requires assumptions to be made about the glue layer that attaches the thin film gage to the test object, and is a significant source of uncertainty in the final heat flux measurement.

The application of Equation 1.1 to thin film gages is shown in Figure 1.2, where  $T_1$  is measured by the RTD and  $T_2$  is measured with thermocouple mounted in the metal test object for the gage developed by Piccini. Direct measurement of the heat flux enables steady-state measurements to be made. For higher frequency measurements a semi-

infinite model can be employed similar to those used on earlier iterations of the gage. Uncertainties are induced in the measurement because a single thermocouple is used for multiple RTDs and a true temperature below each sensor is not measured.

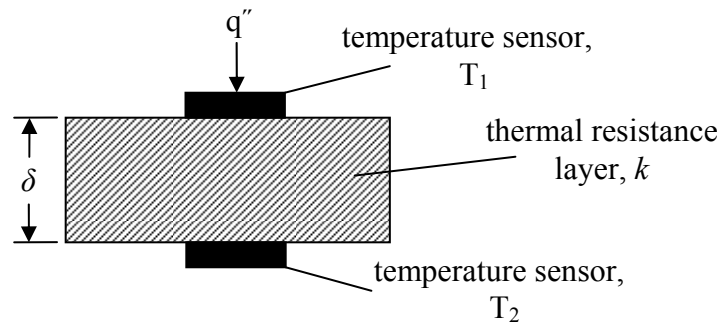


**Figure 1.2.** Diagram of the direct measurement of heat flux.

A second thin-film heat flux array was designed and constructed at MIT [8]. The MIT gage uses platinum RTDs sputtered on either side of a piece of Kapton® to make temperature measurements  $T_1$  and  $T_2$  in Figure 1.2. The gage directly measured the heat flux at low frequencies using Equation 1.1. For high frequency measurements a semi-infinite model was used similar to the one employed by the Oxford group. The MIT gage had calibration problems, as resistances varied over time distorting the temperature measurement from the RTDs.

To extend measurement capabilities beyond that of current thin film arrays, a new type of thin-film heat flux array (HFA) has been developed at Virginia Tech. The HFA is designed to allow direct measurement of the heat flux using nickel/copper thermocouples, which reduces the number of computations required in post-processing and allows for steady-state measurements to be made. Direct measurement also allows the HFA to be mounted on any surface because the model does not incorporate the mounting surface in the heat flux calculation. Another byproduct of direct measurement is that the output of the HFA is only a function of the thermal resistance layer properties and the Seebeck coefficient of the thermocouples. Therefore, once the gage's output has been calibrated, the calibration will remain the same for each of the gages that are produced. Finally, the use of electron beam evaporation to form the thermocouples yields a robust sensor that has consistent output over time.

## Experimental Facilities and Equipment

This section introduces some of the facilities used in the construction and testing of the new Heat Flux Array (HFA) at Virginia Tech. These include: the electron beam (e-beam) evaporation machine that is used to make the HFA, the instrumentation used in the various calibrations performed on the HFA, the convection calibration facility used as

part of the calibration tests, and the digital particle image velocitmetry (DPIV) equipment used for an example application.

## **Thin Film Deposition**

The first step in the deposition of the metals that make up the thermocouples of the HFA is to mount a piece of Kapton® into the vacuum chamber of the e-beam. Then, a graphite crucible is loaded with the metal that is to be evaporated and is placed next to the e-beam gun, which is located in the vacuum chamber below the Kapton® substrate. Next, the chamber is pumped down to a vacuum of  $10^{-6}$  Torr, sufficient enough to bring the substrate within one mean free path of the crucible. The e-beam is activated, and the electrons are guided with electromagnets onto the metal in the crucible which melts and then evaporates. Because the Kapton® is within one mean free path of the crucible, the gaseous cloud of evaporated metal rises and evenly coats the substrate.

The e-beam evaporation facility at Virginia Tech was custom built by Thermionics. The chamber of the machine is twenty-four inches in diameter and is pumped down using a cryogenic pump made by CTI, which is capable of reaching a vacuum of  $10^{-7}$  Torr. The e-beam gun is a five pocket model that supplies up to 3 kV to its filament. The gun has an electromagnetic sweep that moves the beam through the X and Y planes, allowing for even melting of the sample. In addition, an Inficon thickness monitor is mounted in the chamber and uses a water cooled 6 MHz quartz oscillator to measure the deposition rate and total thickness. The thickness monitor measures the frequency of oscillation of the quartz crystal, which changes as metal is deposited on its surface. The density of the metal is used to correlate changes in the crystal's oscillation with the thickness of the film.

## **Instrumentation**

The data collection was done using three different National Instruments (NI) data acquisition systems (DAQs) and Labview. The transient conduction calibration was completed using a 24 bit NI 4351 DAQ sampling at 4 Hz, while the convection calibration was completed using a combination of the TBX and a 24 bit NI USB-9161 thermocouple DAQ. Both of these DAQs were controlled using Labview programs. Since the magnitude of the signal from the HFA is on the order of 40  $\mu$ V, the 24 bits were sufficient to measure the signal.

The time response testing and the test case were completed with a 16 bit NI E-6015 DAQPad. The DAQPad was used so that measurements could be taken at a sampling rate of 3000 Hz, which is beyond the capabilities of current 24 bit systems. The DAQPad does not have anti-aliasing built in, so custom instrumentation was built onto a printed circuit board (PCB) to amplify the signal as well as reduce the possibility of aliasing through the use of a low pass filter that rolls off at 980 Hz. Amplification is applied because the magnitude of a typical signal from the HFA is 40  $\mu$ V and is accomplished using low noise instrumentation amplifiers with a gain of 1000. This increases the

magnitude of the signal read by the DAQ, making it easier to measure as well as providing common mode rejection.

In addition to the amplification and anti-aliasing, the electronics also consisted of a set of resistors that were designed to bleed off excess capacitances that were discovered during testing. After the initial HFA prototype was built and mounted onto a metal plate, it was found that a voltage offset was easily induced in the HFA's output signal when measurements were made with the E-6015 DAQPad and an instrumentation amplifier. This offset was due to the design of the HFA, which when mounted on a plate forms a capacitor as shown in Figure 1.3. Thus, whenever the overall capacitance of the system changed, a voltage offset appeared in the HFA. To counteract this effect, low impedance resistors were placed between the output from the HFA and ground. The ground was then connected to the analog ground of the DAQ. This allowed the charge that had built up in the capacitor to bleed off to ground, rather than saturate the inputs to the amplifier.

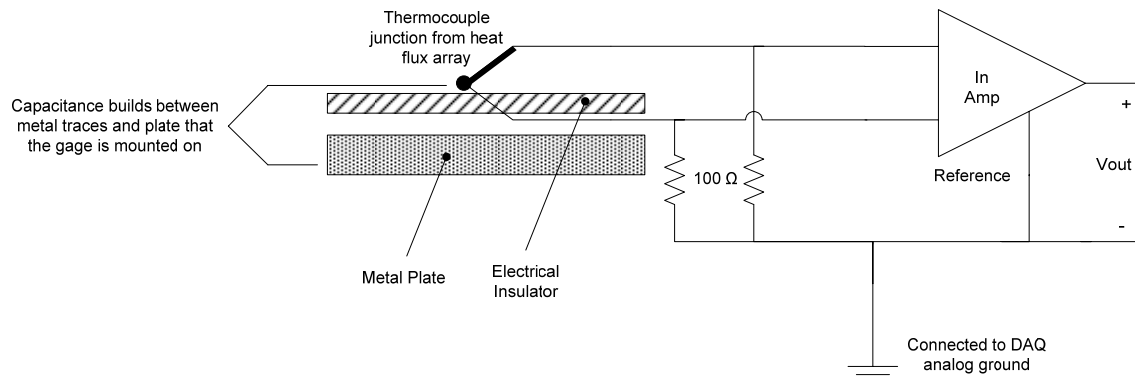


**Figure 1.3.** Diagram of the capacitor built between the HFA and a metal plate. An instrumentation amplifier circuit was designed to amplify the signal while bleeding off the built up capacitance.

## Heat Flux Calibration

The convection calibration was completed by using the convection calibration facility located at Virginia Tech originally discussed by Raphael-Mabel *et al.* [9]. This device is designed around the convection equation for heat flux ( $q''$ ), which is

$$q'' = h(T_\infty - T_s) \quad (1.2)$$

where  $h$  is the convection heat transfer coefficient,  $T_\infty$  is the free stream air temperature, and  $T_s$  is the surface temperature of the gage. The convection calibration facility evenly splits a heated air flow, which then impinges on two flat plates as shown in Figure 1.4. Since the flow is evenly split the resulting convection coefficients are identical on either side of the calibration stand. A Heat Flux Microsensor (HFM) is used as a reference gage to measure the heat flux imparted by the flow stagnating onto one of the plates. The HFM is a fast response point measurement heat flux gage discussed by Holmberg and Diller [10] which is commercially available as a calibrated gage from the Vatel Corporation. The HFM's heat flux measurement is combined with  $T_s$  and  $T_\infty$  from thermocouples TC 1

and TC 2 respectively to yield the convection coefficient from Equation 1.2. With the  $h$  value known, the temperature differential between TC 2 and TC 3 is used to calculate the heat flux through the test gage. The known heat flux is compared with the voltage output of the test gage to yield the sensitivity of the gage in  $\mu\text{V}/\text{W}/\text{cm}^2$ . Modifications were made to the calibration facility discussed in the Raphael-Mabel paper. These modifications included rebuilding the stand for increased rigidity, machining a new t-nozzle to promote mixing and homogeneity in the flow, and redesign of the end nozzles for greater uniformity. All of these changes resulted in an increase in the side to side consistency of the convection coefficient. Comparisons of the output from HFMs mounted on both sides of the test stand demonstrated that there is less than 3% variation in  $h$  side to side.

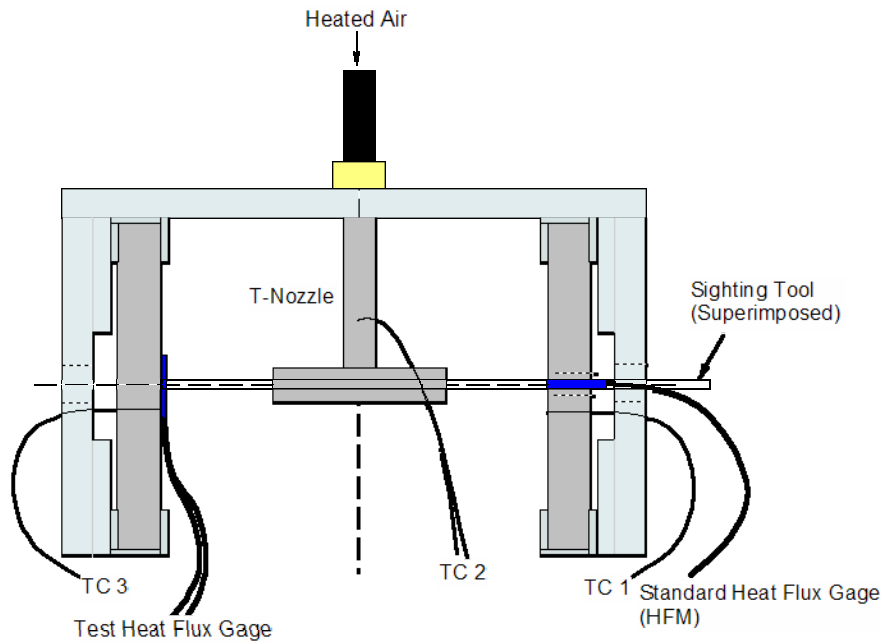


**Figure 1.4.** Diagram of the Convection Calibration Facility at Virginia Tech.

## DPIV Equipment

Digital Particle Image Velocimetry (DPIV) was used to measure the velocity of a flow field stagnating onto a heated flat plate in a water tunnel as an example of the application of the HFA. The time-resolved velocity measurements were then correlated with HFA time-resolved measurements of the heat flux going from the heated plate to the water. To perform DPIV, a flow field is seeded with particles that reflect light when exposed to the laser. Then, the laser is pulsed at a known frequency and digital cameras record images of the particles in the flow field. Software correlates the laser pulses with the change in position of the particles to compute the entire velocity flow field. For further information on PIV methodology, a comprehensive review was completed by Grant [11]. A discussion of DPIV and some of the errors inherent in its application are given by Huang *et al.* [12].

The flow field was illuminated with a Lee Lasers 45W Nd:YAG laser, and a series of lenses and mirrors were employed to focus the beam and then open it again into a thin laser sheet of approximately 1 mm thickness oriented in a plane parallel to the flow direction and perpendicular to the stagnation plate that was used in the example case. The flow was seeded with 11 micron neutrally buoyant glass particles with a specific gravity of 1.1. Motion of the particles was tracked with an IDT XS-5 high-speed camera with a resolution of 40  $\mu\text{m}/\text{pixel}$ . The images from the camera were processed using in-house developed DPIV software [13]. The test section that the stagnation plate was placed into is built of Plexiglas walls which permit optical clarity and help to reduce any three dimensionality of the flow.

## Design of the Heat Flux Array

The Heat Flux Array (HFA) was designed using a differential temperature measurement across a thermal resistance. At steady state Equation 1.1 gives the heat flux. The gage is made by constructing thermocouples on either side of a thermal resistance layer. When the thermocouples are connected through a hole in the thermal resistance layer, as shown in Figure 1.5, the resulting voltage between similar materials is the temperature differential which is directly proportional to the heat flux. The holes act as electrical vias connecting both sides of the resistance layer and are formed by laser drilling the Kapton®. The thermocouples are formed away from the holes so that the differential temperature measurement is not distorted. An additional advantage of using thermocouples is that the traditional temperature measurement on either surface can also be made, as illustrated in Figure 1.5. This is useful in the measurement of flow properties like the convection heat transfer coefficient.

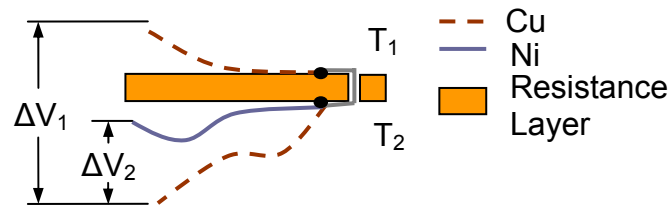


**Figure 1.5.** Thermocouple equivalent circuit of the HFA.  $\Delta V_1$  is a heat flux measurement while  $\Delta V_2$  is a temperature measurement.

Copper and nickel were chosen as the thermocouple materials for the HFA because the combination produces a large Seebeck response [14], which is a measure of the voltage a thermocouple outputs for a given temperature difference. The higher the Seebeck coefficient of the two materials used in the HFA, the greater the heat flux sensitivity will be. In addition to the Seebeck response, both nickel and copper are readily available in bulk wire form and both materials can easily be used in e-beam evaporation. It is convenient to form the thermocouples out of a material that is available as bulk wire to carry the signal back to the DAQ without forming an additional thermocouple junction where the wire is soldered to the gage.

Kapton® was chosen for the thermal resistance layer because it has a low thermal conductivity and is available as a thin film. The low conductivity gives the maximum temperature differential and thus the highest heat flux signal from Equation 1.2. The advantage of using a thin Kapton® film is that the thinner the film is, the less time it takes a thermal signal to be conducted through the film and create a response. The film also allows the gage to be formed to a curved surface, advantageous in mounting the gage in applications such as turbine blade research. Furthermore, Kapton® is a material that is frequently used with copper films in the electronics industry because they adhere well. Since the rest of the gage is made up of metals, Kapton's® melting point sets the theoretical upper temperature limit for continuous use of the gage at 300 °C.

Two different masks were machined using conventional machining practices to form the film into the patterns needed for the HFA. The patterns were designed per experimental requirements. The first mask is a 25 junction array with the junctions evenly spaced in a 5 cm x 5 cm square, while the second is a 10 junction line array with all of the junctions placed 2 mm apart. The finished arrays are shown in Figure 1.6. After the arrays were constructed, wires were soldered onto the gages to allow the signals from the thermocouples to be transferred to the DAQ. The thin copper films necessitated the use of a fluxless soldering process. Flux is designed to dissolve the thin outer layer of copper in order to remove oxidation for the soldering process, and the 0.2 µm film was completely dissolved over time when flux was used.

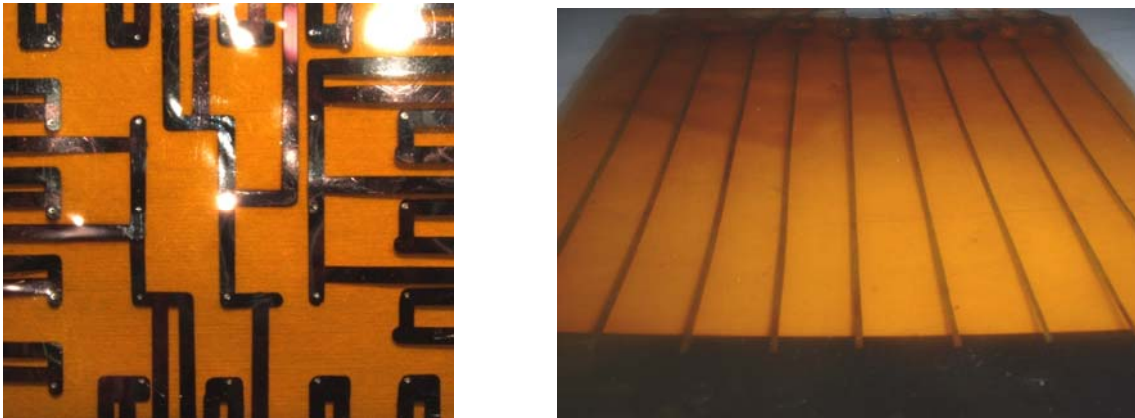


**Figure 1.6.** Pictures of the two junction configurations for the HFA. The 25 junction array is on the left and the 10 junction array on the right.

Once the wires have been soldered onto the HFA, the gage is encapsulated to protect and electrically insulate the gage. The encapsulation is done using a Mylar film, which is 1.5 µm thick. The Mylar is hot pressed onto the HFA using a thermally activated epoxy. The use of thermally activated epoxy allows the glue layer to thin as the hot press heats up and the epoxy cures. This thinning action forces out any air bubbles that may be trapped between the Mylar and the HFA, as well as minimizes the total thickness of the encapsulation layer. Minimization of the encapsulation layer is important because it will affect the thermal resistance of the heat flux gage, which dictates the surface temperature of the gage and could cause error in the measurement of the convection heat transfer coefficient.

It is important to note that since the gage is designed for use in direct measurement, the encapsulation layer does not affect the heat flux gage calibration. The voltage that is output is only dependent on the heat transfer between the thermocouple junctions. The only possible distortion in the output from a calibrated HFA is from degradation of the solder junctions or thermocouples that make up the gage itself. Encapsulation protects the thermocouples from oxidation, and soldering is completed without the use of flux which will destroy the thin copper films.

## Calibration

In order to assess the performance of the heat flux array, a series of calibrations were completed. These calibrations yielded the sensitivity for the heat flux array (HFA) of  $42 \mu\text{V}/(\text{W}/\text{cm}^2)$ , a first order time constant of 32 ms, and a Seebeck Coefficient of the nickel/copper thin film thermocouples of  $23 \mu\text{V}/^\circ\text{C}$ .

A conduction calibration was completed by placing the HFA on top of a Heat Flux Microsensor (HFM), which is the same reference gage used in the convection calibration. Then, a heat flux was applied which was identical through both gages, since they were stacked and the heat flux is one-dimensional and quasi-steady. The outputs were compared to yield the sensitivity of the gage ( $S_{HFA}$ ) in  $\mu\text{V}/(\text{W}/\text{cm}^2)$  by

$$S_{HFA} = \frac{V_{HFA} S_R}{V_R} \quad (1.3)$$

where  $V_G$  is the voltage output by the gage,  $V_R$  is the voltage output by the reference gage, and  $S_R$  is the sensitivity of the reference gage. A plot of the output from a transient conduction test is shown in Figure 1.7. The plot shows the output from the HFM compared with the output from the HFA. Both gages show the typical transient conduction heat flux curve, which decays with time. The calibrated sensitivity, which is plotted on the right axis, remains nearly constant as expected. There is a difference in the output of the gages from test to test because the heat flux source was not constant. However, the calibrated sensitivity of the HFA is proportional to the ratio of the two signals and should remain constant between tests.

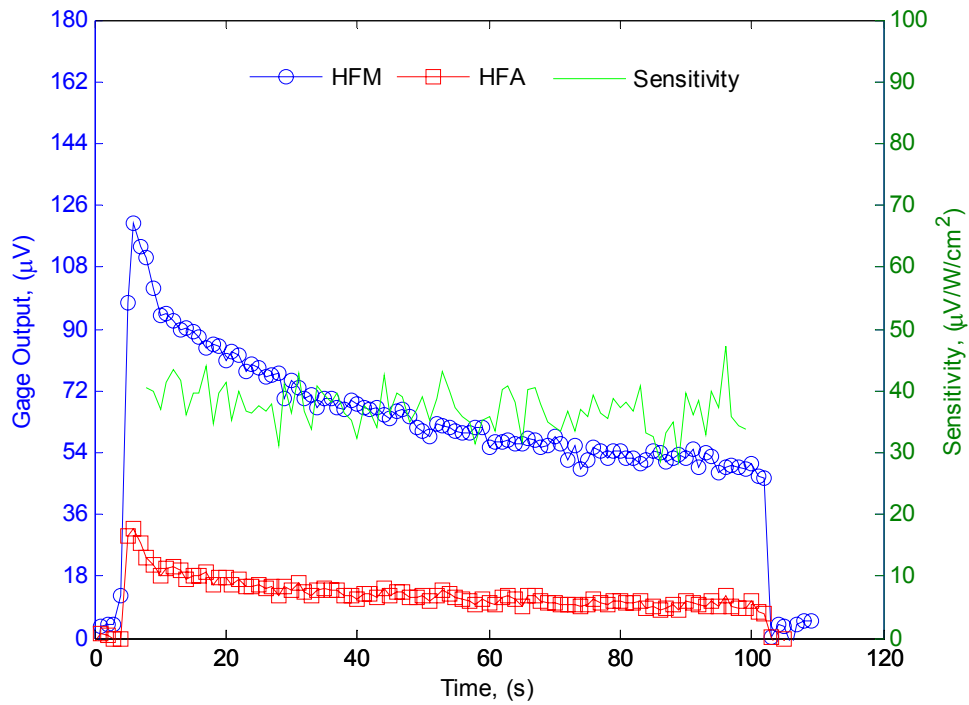


**Figure 1.7.** Plot of the output from a conduction test.

The transient conduction test was run on five different junctions. The heat flux was applied through each side of the gage and each junction was tested twice. This resulted in a total of 20 tests and the average values from each run are shown in Figure 1.8. The average sensitivity over all of the test runs was  $41.8 \pm 2 \mu\text{V}/(\text{W}/\text{cm}^2)$ . The uncertainty in the calibration is estimated using the techniques outlined in the NIST Technical Note 1297 [15]. The 95% confidence interval for the data is  $14 \mu\text{V}/(\text{W}/\text{cm}^2)$ .

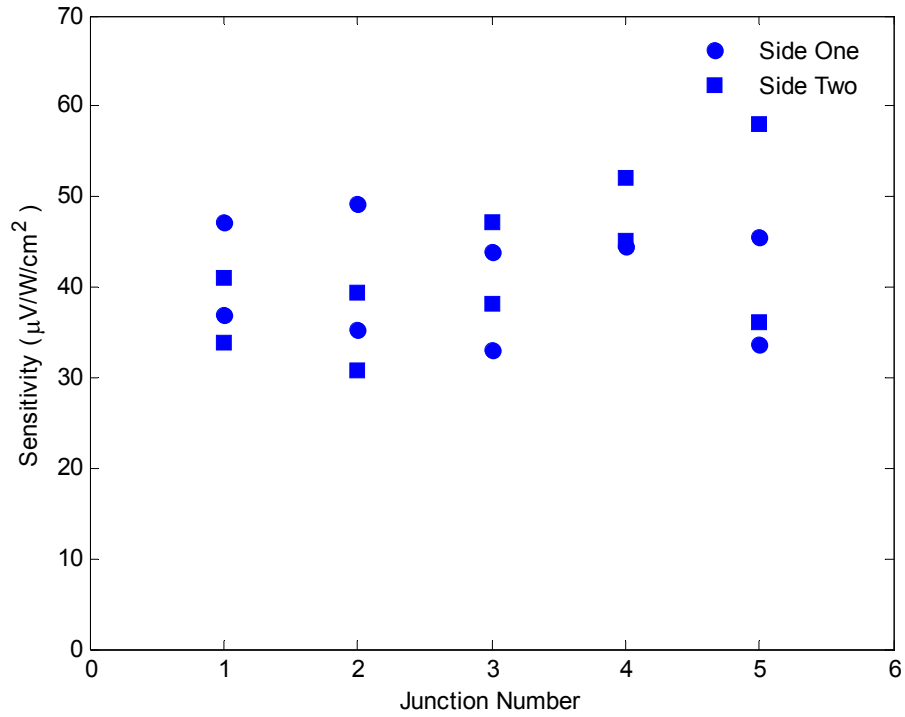


**Figure 1.8.** Summary of the resulting sensitivities from the transient conduction test.

The convection calibration stand was used to augment the results from the transient conduction test. The convection stand was run over a series of different line pressures resulting in seven different nozzle flow rates and therefore seven  $h$  values for a single junction of the HFA. The sensitivity was computed over the duration of each test neglecting the added thermal resistance of the HFA and the average value was calculated and is plotted in Figure 1.9. The average of the sensitivity values from each run is  $42 \pm 3 \mu\text{V}/(\text{W}/\text{cm}^2)$ , where the error is the 95% confidence interval for all of the tests.

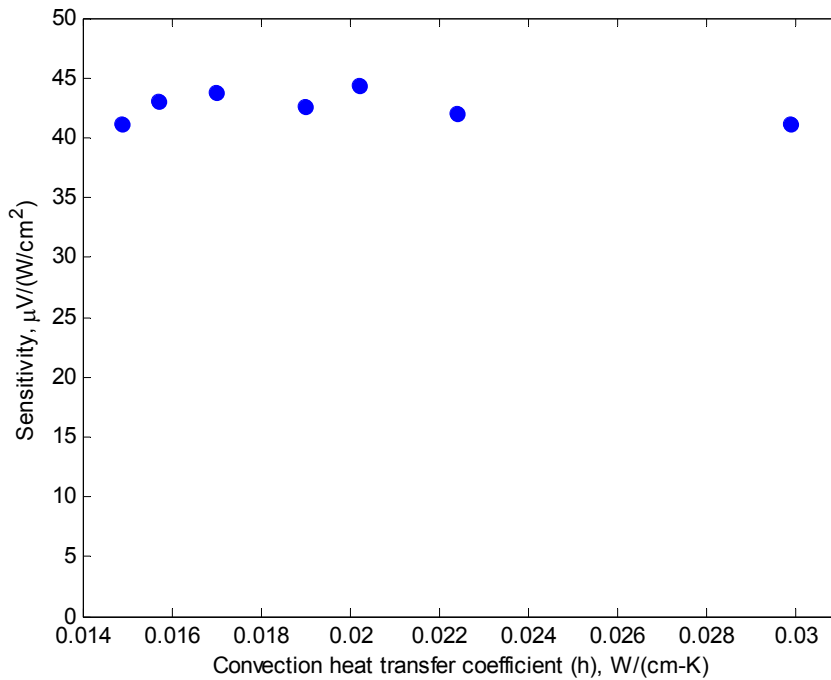


**Figure 1.9.** Results curve from the convection calibration facility.

The sensitivity of the HFA is a result of two factors, the material properties of the resistance layer and the thermoelectric response of the thermocouple pairs that make up the heat flux gage. Since a traditional bulk wire thermocouple was not used, the Seebeck coefficient of the nickel/copper thin film thermocouples was measured. The Seebeck coefficient ( $Se$ ) is the output of the thermocouple when exposed to a temperature differential ( $\Delta T$ ) and is found by

$$Se = \frac{V_o}{\Delta T} \quad (1.4)$$

where  $V_o$  is the voltage output by the thermocouple. An experiment was set up based upon Equation 1.4 where the temperature differential was imposed onto a test specimen as shown in

Figure 1.10. Wires were soldered onto the specimen as shown in the figure and voltages were measured at different temperature differentials using a multimeter. Using thermocouples to measure the temperatures, the Seebeck coefficient was then calculated from Equation 1.4 with the results shown in Figure 1.11. The coefficient for the copper film is close to zero, as would be expected from theory. The nickel/copper junctions have an average Seebeck coefficient of  $23 \pm 0.7 \mu\text{V}/^\circ\text{C}$ , which closely matches the theoretical values for bulk copper [14]. The uncertainty is estimated using the same NIST method as the previous calibrations [15].

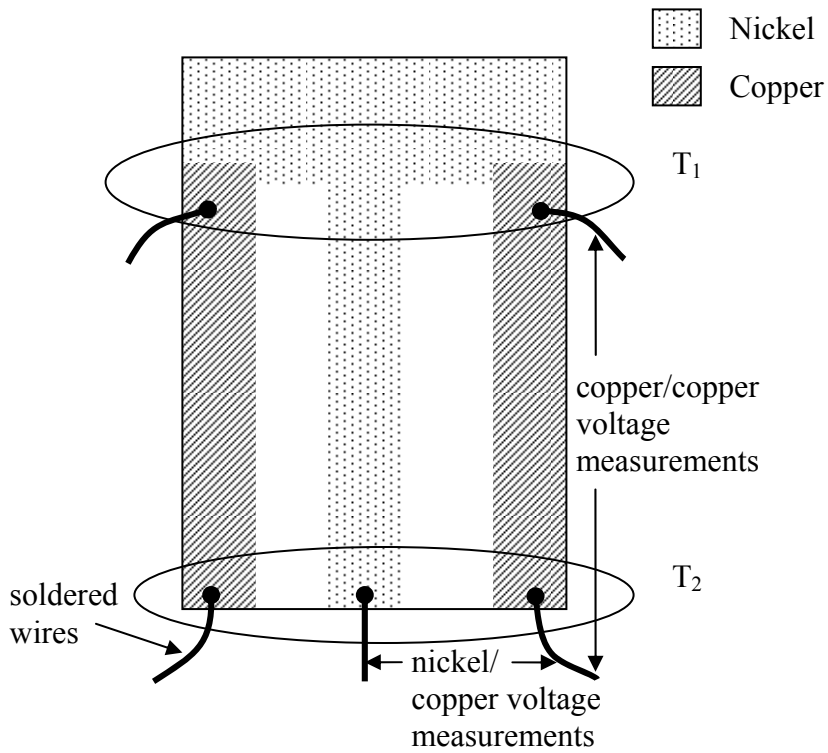


**Figure 1.10.** Diagram of the HFA used in the Seebeck experiments.

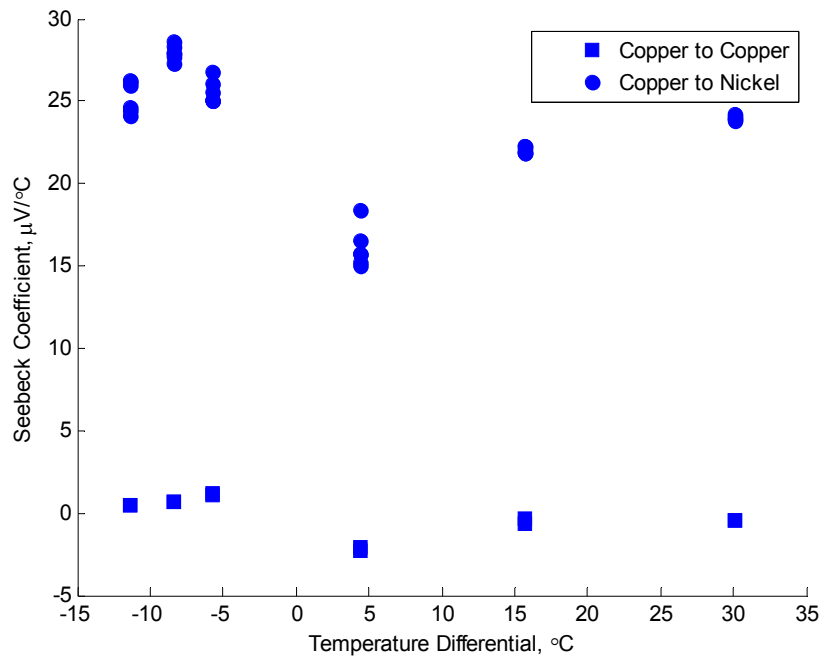


**Figure 1.11.** Results from the Seebeck coefficient experiment.

The results from the sensitivity and Seebeck calibrations can be further analyzed to obtain information about the gage and the materials used in its construction. Equation 1.4 can be combined with Equation 1.1 to yield the thermal conductivity of the Kapton® ( $k$ )

$$k = \frac{\delta}{S_{HFA}} Se \quad (1.5)$$

where  $\delta$  is the thickness of the Kapton®. Substituting the measured Seebeck coefficient for nickel/copper thermocouples of  $23 \mu\text{V}/^\circ\text{C}$  into Equation 1.5 along with the average sensitivity of the HFA of  $40 \mu\text{V}/(\text{W}/\text{cm}^2)$  results in a thermal conductivity of  $0.288 \text{ W}/(\text{m}\cdot\text{K})$ . This is twice the reported value of most types of Kapton® [16]. Type E Kapton® film was used in the construction of the HFA, and thermal conductivity values for this film were not reported. Therefore, the Type E films appear to have roughly twice the thermal conductivity of other Kapton® films.

The time response of the HFA was found by using a laser pulsing at 10 kHz to input a step heat flux signal into the gage. An assumption was made that the gage would not respond faster than 10 kHz, and that the laser's pulse would be time averaged into a quasi-steady step input. The gage's output was sampled at 3000 Hz with hardware aliasing filters. The response was then digitally low pass filtered at 1000 Hz, and notch filters were used at 60 Hz and its harmonics for noise removal. The resulting signal is shown in Figure 1.12, and as predicted the pulse of the laser is time averaged and does not distinctly appear in the signal. Examination of the gage's response to a step also showed that the gage returned to a zero value when the heat flux was removed from the gage. This shows that the gage's response is linear, and that hysteresis error is minimal.

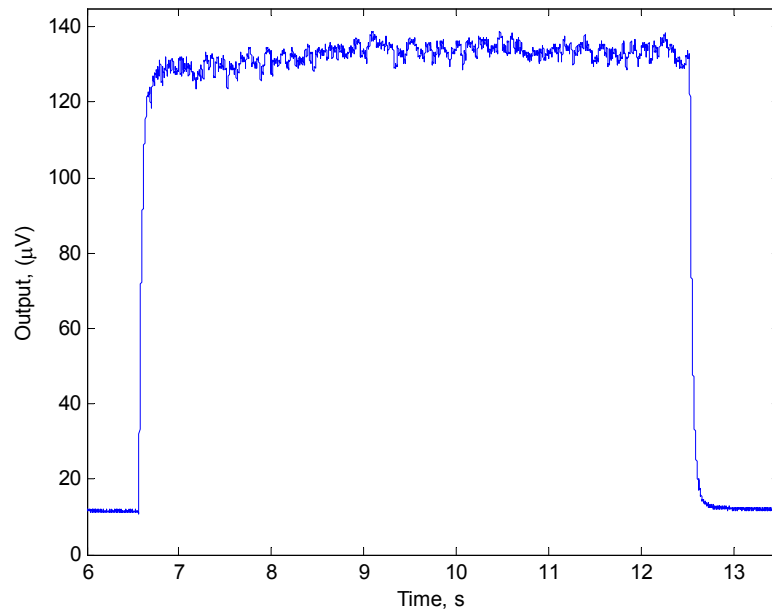


**Figure 1.12.** Response of the HFA to a step input.

In order to create the step, a metal obstacle was placed in front of the laser, and then removed. Since the obstacle was moved by mechanical means, there was a short period of time where the gage did not see 100% of the heat flux output by the laser, meaning that the step was actually a ramp. The obstacle was placed close to the focal point where the beam diameter was less than 1 mm. The obstacle was moved at approximately 40

cm/s, which meant that the HFA was exposed to a partial heat flux for 2.5 ms. This was taken into consideration in the estimation of uncertainty that was completed for the HFA.

To quantify the response of the HFA, the rise and fall of the output signal was investigated. An average value was taken for a short time period before and after the step as shown in Figure 1.13, so that the magnitude of the step could be found. Then, the time that it took the HFA's response to reach 63% ( $1-e^{-1}$ ) of the full value was calculated. For the fall time the same steps were taken, but in reverse. For a 50  $\mu\text{m}$  Kapton® resistance layer, both the rise and the fall showed similar values as reported in Table 1.1. The average response time for the HFA was found to be  $32 \pm 3$  ms, where the uncertainty was estimated using the guidelines developed by NIST [15] and the 95% confidence interval for the measurements is 4 ms. The results validate the initial assumption that the gage could not pick up the individual pulses in the laser.

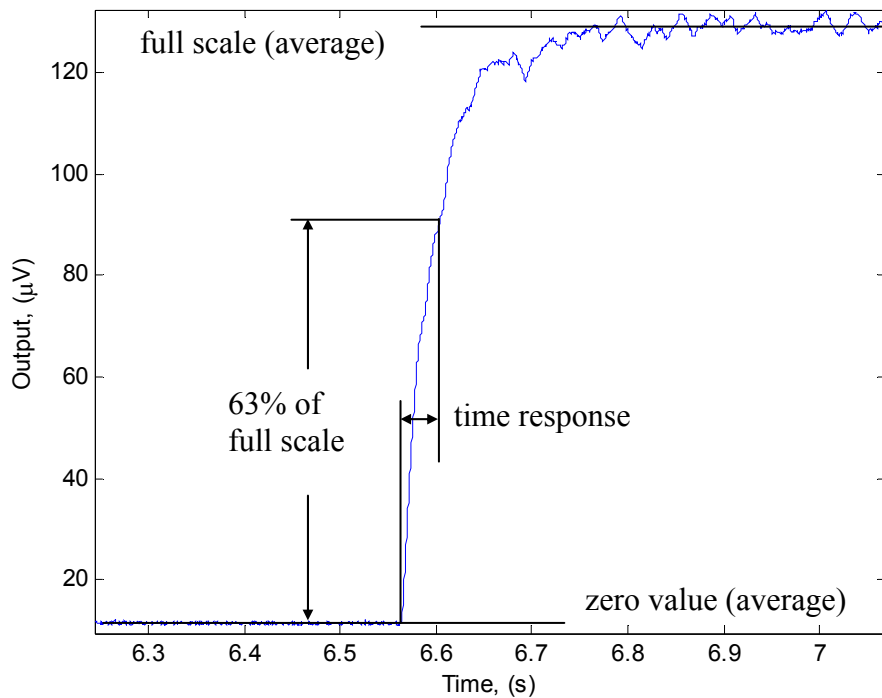


**Figure 1.13.** Zoomed view of the response of the HFA to a step input from Figure 1.12.

**Table 1.1.** Table of the rise and fall times for five runs of the time response test.

Run No.	Rise (ms)	Fall (ms)	Average (ms)
1	31.7	30.0	30.9
2	30.7	36.0	33.4
3	33.0	33.0	33.0
4	32.7	33.3	33.0
5	31.7	35.0	33.4

## Test Case

A sample of results for a research application of the HFA is presented here as a test case showing one way in which the gage can be used.

The experiment is designed to study the time-resolved effects of free stream turbulence on heat transfer in stagnating flow. This is done by creating grid turbulence in a water tunnel, which then interacts with stagnating flow on a flat plate placed normal to the flow. The plate is heated using a resistance heater, creating a heat flux from the plate into the flow. The HFA was used to measure the time-resolved heat flux, which was then correlated with the time-resolved velocity of the flow that was measured using the PIV system described earlier.

The PIV results yielded an entire turbulent flow field, which was correlated to the heat flux. Correlation was done with both the  $u'$  and  $v'$  components of the velocity field, which are respectively streamwise and perpendicular to the flow. For a flow with a free stream velocity of 10 cm/s, a sample of the fluctuating values of the heat flux and  $u'$  velocity component at the stagnation point are as shown in Figure 1.14. The heat flux follows the trend of the velocity as the fluid moves in and transfers thermal energy with the surface of the stagnation plate. These results not only tell something about the transfer of energy in a turbulent flow field, but are a good demonstration of a case where the capabilities of the HFA can be put to good use.

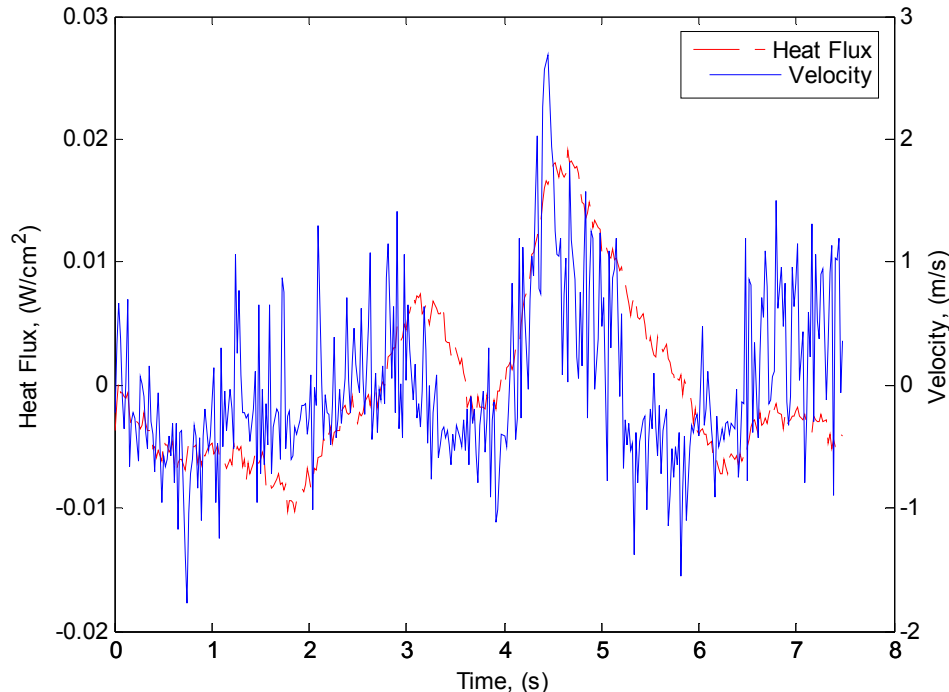


**Figure 1.14.** Heat flux and velocity results for turbulent flow stagnating on a flat plate.

## Conclusions

A thin-film heat flux array (HFA) has been developed that expands the capabilities of currently available heat flux measurement technology. It has already been used in a research application to measure time-resolved heat flux in turbulent flow. The array utilizes a direct measurement technique that allows it to be placed on any surface. As a result of encapsulation, the array can be used to take heat flux measurements in any fluid. In addition, use of thin-film technology gives the array a first order time constant of 32 ms for arrays built with a 50  $\mu\text{m}$  Kapton® resistance layer. Calibration of the array yields an average sensitivity of 42  $\mu\text{V}/(\text{W}/\text{cm}^2)$ , which is sufficient output for most applications. In order to boost the signal and counteract capacitance effects inherent to the gage's design, a custom bank of electronics has been designed.

## References

1. Kidd, C.T. and Adams J.C, Jr., "Fast-response heat-flux sensor for measurement commonality in hypersonic wind tunnels". *Journal of Spacecraft and Rockets*, 2001. **38**(5): p. 719-729.
2. Schultz, D.L. and T.V. Jones, "Heat-Transfer Measurements in Short-Duration Hypersonic Facilities". *AGARDograph*, 1973(165): p. 149.
3. Doorly, J.E. and M.L.G. Oldfield, "Theory of Advanced Multi-Layer Thin Film Heat Transfer Gauges". *International Journal of Heat and Mass Transfer*, 1987. **30**(6): p. 1159-1168.
4. Ainsworth, R.W., et al., "Developments in instrumentation and processing for transient heat transfer measurement in a full-stage model turbine". *Journal of Turbomachinery*, 1989. **111**(1): p. 20-27.
5. Anthony, R.J., T.V. Jones, and J.E. LaGraff. "Unsteady surface heat flux under a three-dimensional crossflow boundary layer". 2004. Reno, NV, United States: American Institute of Aeronautics and Astronautics Inc., Reston, United States.
6. Anthony, R.J., T.V. Jones, and J.E. LaGraff, "High frequency surface heat flux imaging of bypass transition". *Journal of Turbomachinery-Transactions of the Asme*, 2005. **127**(2): p. 241-250.
7. Piccini, E., S.M. Guo, and T.V. Jones, "The development of a new direct-heat-flux gauge for heat-transfer facilities". *Measurement Science & Technology*, 2000. **11**(4): p. 342-349.
8. Epstein, A.H., et al., "High-Frequency Response Heat-Flux Gauge". *Review of Scientific Instruments*, 1986. **57**(4): p. 639-649.
9. Raphael-Mabel, S., et al. "Design and calibration of a novel high temperature heat flux gage". 2005. San Francisco, CA, United States: American Society of Mechanical Engineers, New York, NY 10016-5990, United States.
10. Holmberg, D.G. and T.E. Diller, "High-frequency heat flux sensor calibration and modeling". *Journal of Fluids Engineering, Transactions of the ASME*, 1995. **117**(4): p. 659-664.
11. Grant, I., "Particle image velocimetry: A review". *Proceedings of the Institution of Mechanical Engineers, Part C: Journal of Mechanical Engineering Science*, 1997. **211**(1): p. 55-76.

12. Huang, H., D. Dabiri, and M. Gharib, "On errors of digital particle image velocimetry". *Measurement Science & Technology*, 1997. **8**(12): p. 1427-1440.
13. Abiven, C. and P.P. Vlachos. "Super spatio-temporal resolution, Digital PIV system for multiphase flows with phase differentiation and simultaneous shape and size quantification." 2002. New Orleans, LA, United States: American Society of Mechanical Engineers, New York, NY 10016-5990, United States.
14. Diller, T.E., "Advances in Heat Flux Measurements, in *Advances in Heat Transfer*", J.P. Hartnett and T.F. Irvine Jr., Editors. 1993, Academic Press: Boston. p. 279-368.
15. Taylor, B.N. and C.E. Kuyatt, "Guidlines for Evaluating and Expressing the Uncertainty of NIST Measurement Results." 1994, Physics Laboratory, National Institute of Standards and Technology: Gaithersburg, MA.
16. Dupont. "Summary of Properties of Kapton Polyimide." [cited 2006; Available from:  
[http://www2.dupont.com/Kapton/en\\_US/assets/downloads/pdf/summaryofprop.pdf](http://www2.dupont.com/Kapton/en_US/assets/downloads/pdf/summaryofprop.pdf).

## Appendix A: Construction of the Heat Flux Array

The e-beam used in construction of the Heat Flux Array (HFA) is owned by the MicrON group at Virginia Tech, and they require that all users complete training. It is assumed that any individual who will be constructing HFAs will have gone through this training process and know the basics of e-beaming. Details of operation specific to the construction of the HFA are given here, as well as some basic principles that may not be emphasized in the training. A picture of the e-beam is shown in Figure A-1 to serve as a general guide to the location of the components mentioned in the Facilities section, as well as the discussion in this Appendix.

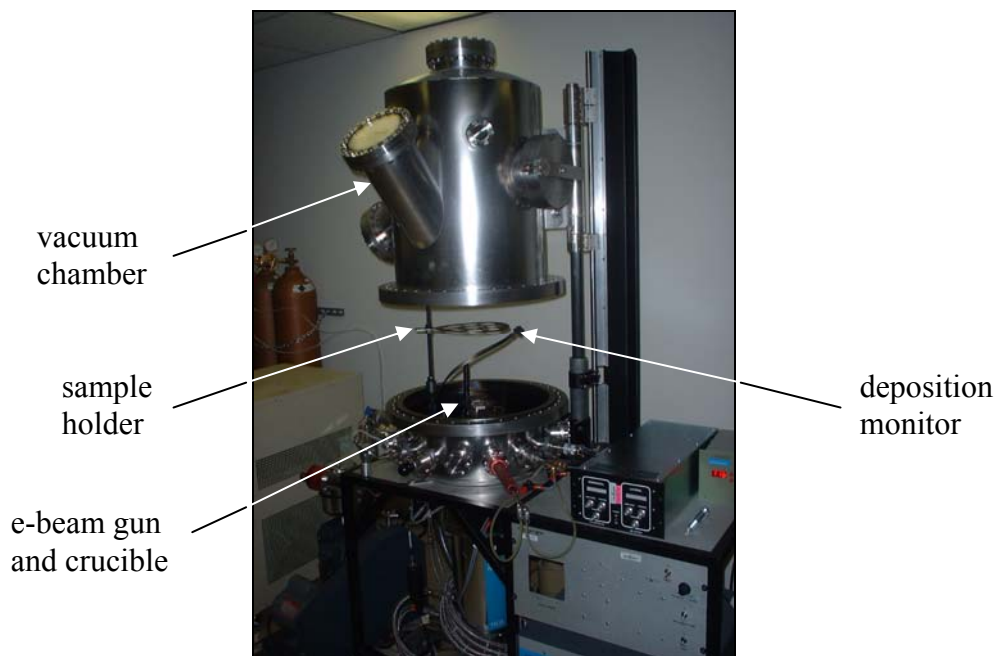


**Figure A.1.** The e-beam facility.

The HFA goes through several stages of construction. First, a piece of Kapton® is prepared by laser drilling the holes into it that form the vias that connect the nickel on either side, as shown in Figure 1. The laser drilling is done in the CPES Packaging lab using a CO<sub>2</sub> laser with a two-axis CNC control by Dan Huff. After the Kapton® is drilled, it is cleaned in preparation for the e-beam. Then, the proper mask is selected depending on the pattern that needs to be e-beamed onto the Kapton® substrate. The masked substrate is then placed into the chamber and e-beamed. After the e-beaming is completed, wires are soldered onto the array, and finally it is encapsulated to form the finished product

The Kapton® is cleaned by washing it in Acetone, Isopropanol (IPA), and then deionized (DI) water. The rinse removes all of the greases and oils that might be present on the Kapton® so that they will not outgas during the evaporation process and contaminate the

films. Care should be taken to ensure that the surface of the Kapton® is as clean as possible. In order to facilitate the drying of any cleaned materials, lint free cloths are used to wipe them dry. Any new masks or other pieces of metal that are to go into the e-beam must be cleaned using this procedure. Standard zip lock sandwich bags are used to protect the cleaned items until they go into the e-beam.

Once the Kapton® is cleaned, it must be masked for the e-beam chamber. Three sets of masks currently exist. Two sets that create the patterns shown in Figure 2, and one set that was used to create a prototype of the HFA. The masks were constructed using a mill to mill out the desired patterns. Experiments have been completed to determine if a mask could be made by laser drilling 200 micron slots into a sheet of Kapton®. The laser drilled Kapton® mask creates a pattern of vertical lines that are spaced close together. However, the durability of the traces has not been tested and some development work would need to be completed to ensure that a gage made from a Kapton® mask will last through an entire experiment.

To mask the Kapton®, it is mounted onto an aluminum plate using Kapton® tape. This is done to heat sink the Kapton®, preventing localized burning during the deposition process. Once the Kapton® has been taped onto the heat sink, the mask is taped over the Kapton® to get the desired pattern. After the mask and Kapton® have been mounted on the aluminum heat sink, it's placed on an aluminum sample holder, shown in Figure A.2. The sample holder has a hole that allows the Kapton® and the mask to be exposed to the evaporated metal. The slot is placed into a threaded rod in the e-beam, and washers and nuts are tightened on either side to hold the holder in place. The sample holder is positioned so that the Kapton® is as far away from the crucible in the center of the chamber as possible (reference Figure A.1). This is to minimize the effect of radiation from the metal in the crucible to prevent burning of the Kapton®. In order to increase operating efficiency, it may be desired to design a new holder that could be used to construct two or three arrays at the same time.

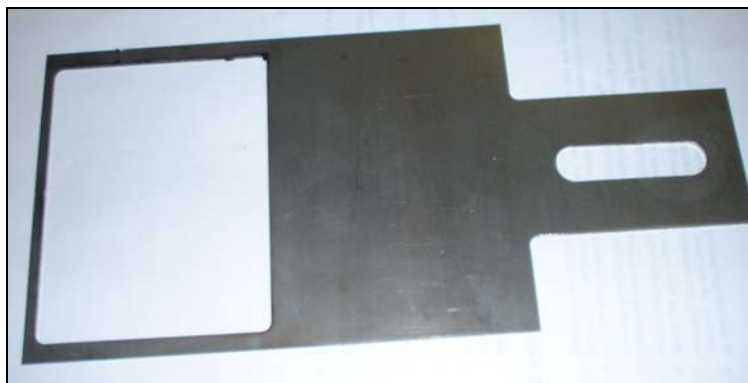


**Figure A.2.** The holder that supports the heat sink and substrate in the e-beam.

When the Kapton® has been mounted into the chamber, the chamber is evacuated and pumped down to a pressure of at least  $3 \times 10^{-6}$  Torr. The purpose of reaching the high vacuum is to bring the substrate within one mean free path of the gaseous metals that are evaporated from within the crucible. Therefore, performing a deposition when the proper

vacuum has not been reached will result in contaminated films that may not have the properties that are desired. If the cryo pump cannot reach the desired vacuum, it is likely that the rubber seal that seals the chamber needs to be changed.

The actual deposition of the metals is fairly straightforward. Copper is easy to deposit, as it melts at relatively low temperatures. Therefore, the standard evaporation procedure can be employed. With the MicrON e-beam, copper should evaporate at approximately 100 mA. This value will vary slightly depending on the base pressure that the evaporation is performed at. Nickel, however, raises some challenges in its deposition. Nickel requires more current, because it has a higher melting temperature, approximately 150 mA. Furthermore, nickel is magnetic. This means that the electromagnets that are usually used to control the e-beam cannot be used, as the nickel will influence their magnetic field, causing the beam to act in an odd manner. It is suggested that an experienced user assist in the deposition of nickel at least once.

If it is observed that either of the materials requires currents substantially (~50 mA) higher than normal at typical evaporating pressures of  $2 \times 10^{-6}$  Torr, that means that the crucible has become contaminated. This is caused by the graphite, which is what the crucibles are made of, working its way into the base material located in the crucible. Typically, visual inspection can verify that a crucible is contaminated. The metal in a clean crucible will appear smooth, like the crucible in the right of Figure A.3. The crucible on the left is typical of a contaminated crucible. The surface becomes pitted as the metal becomes inhomogeneous and evaporates at different temperatures. In addition, a dull grey color will begin to appear as the graphite works its way into the metal.

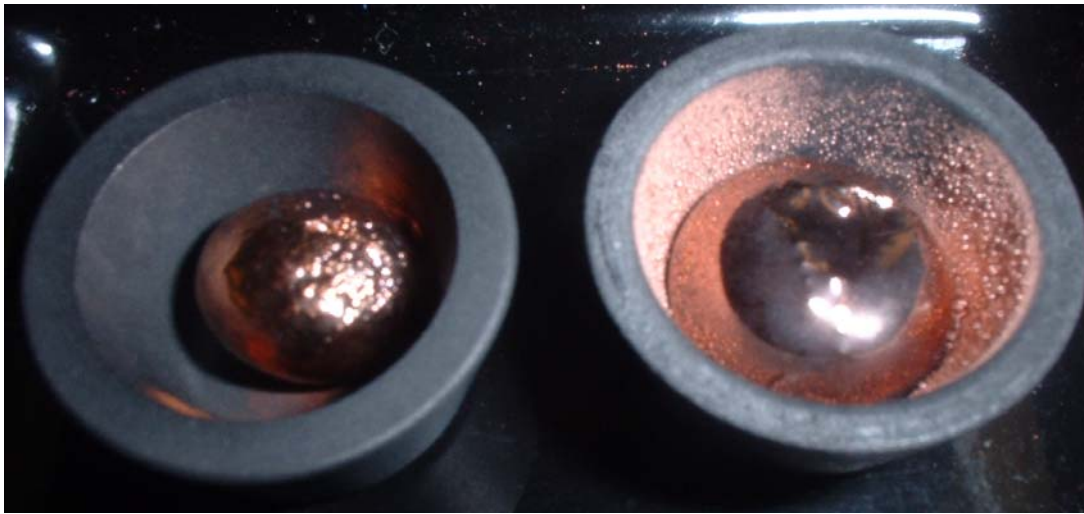


**Figure A.3.** Photograph of the crucibles used in e-beam evaporation. A contaminated crucible is on the left, while a clean crucible is on the right.

When a crucible is contaminated, the base material can either be cleaned or discarded. The cleaning process consists of taking the base material and soaking it in HCl. This process will remove the graphite, and can be used for copper which turns into a ball when evaporated. However, since nickel adheres to the crucible the entire nickel crucible must be discarded and a new one started.

After the deposition of the thin films is complete, 36 gage wires are soldered onto the HFA's leads. The wires are soldered using a fluxless soldering process. This is done because the flux will disintegrate the thin copper films that are used in the construction of the HFA. If the films were 2-3 microns thick, flux may be able to be used, as long as it was promptly and thoroughly cleaned. The purpose of flux in the soldering process is to deoxidize the metals that are going to be soldered. Therefore, to solder without flux, a deionized water/HCl solution is used to deoxidize the films, the solder, and the wires. 62 Sn 36 Pb 2 Ag ribbon solder from Indium Corporation is used as the solder. When everything has been deoxidized, the solder tape is wrapped around the wires, and then the wires and the Kapton® are taped onto a piece of ceramic. The ceramic provides stability during the soldering process, and enables the entire package to be placed on a hot plate, which is set at 180 °C. The hot press warms up the package, and prepares the solder to flow easily. A soldering iron which is set at 700 °C is then used to melt the solder, which should flow along the length of exposed signal wire.

As soon as the soldering is complete the HFA is hot pressed to protect it from shorting out when it is mounted onto a metal surface as well as minimize the oxidation of the copper films when exposed to air. It is recommended that the soldering and hot pressing processes be completed on the same day, again to counteract the effects of oxidation. Ideally, the HFA should be taken out of the e-beam chamber, soldered, and then hot pressed.

The gage is hot pressed using a thermally activated epoxy from the John C. Dolph company. This allows the press to squeeze out as many air bubbles as possible while the epoxy cures. To hot press a HFA, the gage is first cleaned with Acetone to remove any greases and oils that may have developed onto the gage. Then, the gage is mounted into the hot press along with the epoxy and Mylar, which is a plastic film used to encapsulate the gage. The Mylar is spread taut using Kapton® tape at all of the corners to hold it down. In order to squeeze out the air bubbles in the glue layer, the gage, epoxy, and Mylar are sandwiched with Teflon as shown in Figure A.4. The Teflon pyramid will form a void once everything is pressed that the glue and air bubbles will be forced into. The gage is pressed at 300 °F for 8 hours. Once the press has cooled, any excess Mylar is trimmed from around the gage.

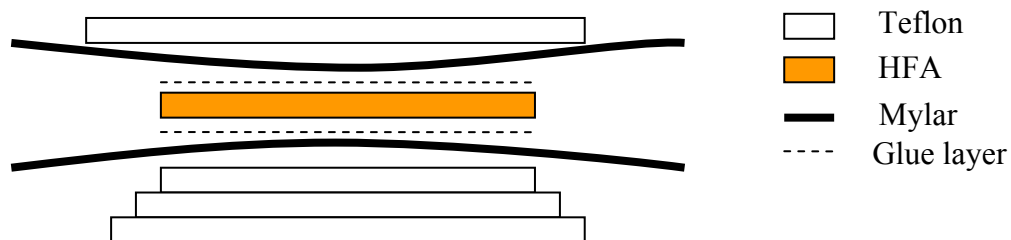


**Figure A.4.** Diagram of the stack that is inserted into the hot press.



The main reason that the circuit boards were designed and made was so that a low noise amplifier could be selected for the amplification. In addition to a low noise floor, the amplifier had to be capable of amplifying a microvolt signal into the range where it could be measured using a 16-bit DAQ board. The equation used to determine the DAQ's resolution ( $V_{min}$ ) is

$$V_{min} = \frac{\Delta V}{2^n} \quad (B-1)$$

where  $\Delta V$  is the input range for the DAQ and  $n$  is the number of bits. With the DAQpad used in the HFA experiments, the input range used is  $\pm 500$  mV. Since the DAQpad is a 16-bit DAQ, its resolution by Equation A-1 is  $15 \mu\text{V}$ . Allotting for noise in the DAQ and amplifier, it was decided that a gain of 1000 would be used for maximum resolution of the signal.

The Analog Devices AD624 instrumentation amplifier was chosen for use in the PCB. The AD624 selected because it is capable of 1000 gain, and had a noise specification of  $0.2 \mu\text{V}$  peak to peak at low frequencies (low in comparison to other amplifiers). An added feature of the AD624 is that it has internal laser trimmed resistors that are used to set the gain. The advantage of this feature is that the gain fluctuates much less over time, and is easier to use than the type of amplifier that requires an external resistor to be hooked up to specify the gain. The final specification investigated in the selection of an amplifier was the common mode rejection ratio (CMRR). This measures how well the amplifier rejects a signal common to both inputs and is typically used in the cancellation of electrical noise. The CMRR for the AD624 is 130 dB at 60 Hz, which means that 130 dB of the common mode content at 60 Hz will be suppressed.

Currently, the board is designed so that the gain of each channel must be tested for individually. The AD624 provides a set of pins which allow for gain correction. Further board development would include a design which would allow the user to test each amplifier before it was attached to the PCB, and determine its gain. Then, a set of resistors could be added to the PCB which would correct the amplifiers gain to exactly 1000. This would negate the need for testing of each channel, and the application of a gain matrix to whatever data is collected.

The signal from the heat flux gage is a differential signal between two thermocouples. Therefore, the amplification circuit is set up as a floating differential measurement. The gage's signal is input into the amplifier, which outputs the magnitude of the difference as a voltage value between the amplifier's output and reference pins. The reference pins of the amplifiers are all tied to a common ground and are connected to the negative output on each of the channels. Therefore, to make a measurement using a DAQ in the differential measurement configuration the positive output pin for each channel should go to the positive input on the DAQ, the negative output pin should go to the negative input pin on each channel, and one of the negative input pins should be connected to the analog ground on the DAQ. To make a single ended measurement, one of the negative inputs should be hooked into the analog sense pin, and the positive output from each channel

should be connected to the each channel input. A synopsis of the signal hookups is given in Figure B.3.

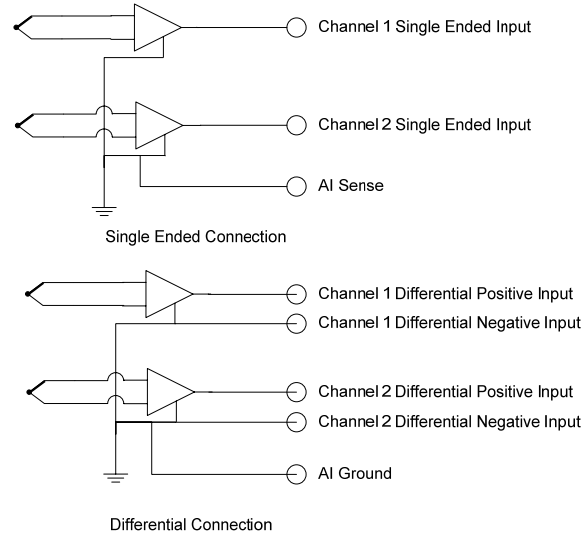


**Figure B.3.** Diagram of the DAQ connection for use with the measurement system. The capacitors and anti-aliasing filters are not shown.

In order to guarantee a clean power supply for the amplifiers, a two custom-made battery packs were purchased. One is the positive supply and one is the negative supply. A battery pack is made up of 14 1.2V nickel-metal cells with a total capacity of 1600 mW-hrs. The battery packs are capable of several hours of service before they need to be recharged. The pack voltage of 16.8 V is close to the maximum rating of the AD624 which is 18 V. Therefore, care should be taken in monitoring the battery pack voltage to ensure it doesn't exceed 18 V. In addition, the voltage of the battery packs which are the negative and positive supply should not differ by more than half a volt. This is to protect the instrumentation amplifiers and to keep the circuit balanced. Voltages of less than 15 V will cause the amplifiers to perform at less than their rated value for CMRR. Thus, if the battery packs begin to display voltages of less than 15 V they should be recharged.

Besides amplification, the PCBs are also used for anti-aliasing. Aliasing results when frequency content is faster than the sampling rate of the DAQ. The digitized points will appear to be a lower frequency, even though they are actually a high frequency, as shown in Figure B.4. Aliasing was a problem early in the design stages of the HFA, as the aliasing caused a broadband noise that hid the heat flux signal. A first order RC filter provided enough of a cutoff to reduce aliasing. The RC filter was designed with a cutoff frequency of 980 Hz so that the data could be sampled at 3000 Hz and still provide the necessary information. The cutoff frequency,  $f_c$  can be found by

$$f_c = \frac{1}{2\pi RC} \quad (\text{B-2})$$

where  $R$  and  $C$  are the values of the resistor and capacitor respectively. A possible improvement for the aliasing filtering would be to use a second or third order active filter that would roll off quicker and provide better filtering. However, to obtain a higher order

filter op amps would have to be used which would add to the complexity of the board and increase the power requirements.

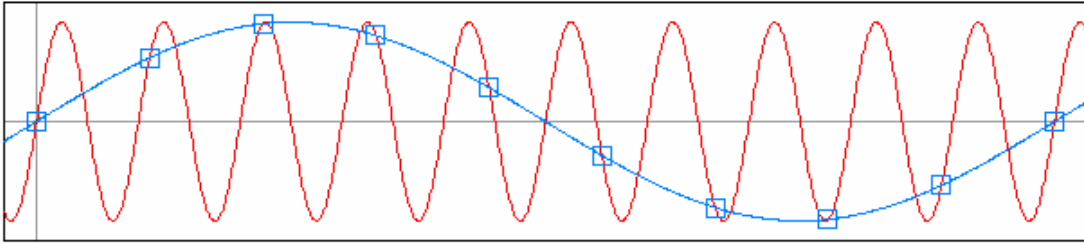


**Figure B.4.** Diagram of an aliased signal.

## Appendix C: Uncertainty Estimation

The uncertainties of the tests in this thesis were estimated using the standards set forth by the National Institute of Standards and Technology (NIST) in technical note 1297 [15].

### Conduction Calibration Uncertainty

The uncertainty of the conduction calibration is based upon the equation for the sensitivity of the HFA. From Equation 1.3, the sensitivity of the HFA is

$$S_{HFA} = \frac{V}{q''} \quad (C.1)$$

The sources of error in the measurement are the error in the heat flux measured by the HFM and the error in the HFA's output voltage measurement. These can be analyzed with the formula for the propagation of error to yield the combined uncertainty ( $u_c$ )

$$u_c = \sqrt{\left(\frac{\partial S_{HFA}}{\partial q''}\right)^2 u_q^2 + \left(\frac{\partial S_{HFA}}{\partial V}\right)^2 u_v^2} \quad (C.2)$$

where  $u_q$  is the uncertainty in the heat flux measurement and  $u_v$  is the uncertainty in the voltage measurement. The partial derivatives are known as the sensitivity coefficients. Evaluation of the sensitivity coefficients from Equation C.1 results in the final equation for the uncertainty in the sensitivity

$$\frac{u_c}{S_{HFA}} = \sqrt{\left(\frac{1}{q''}\right)^2 u_q^2 + \left(\frac{1}{V}\right)^2 u_v^2} \quad (C.3)$$

The error budget in Table C.1 is used to determine  $u_q$  and  $u_v$  by taking the square root of the sum of the squares of uncertainty in each of the measurements. Using MATLAB, Equation C.3 was solved and then averaged for each conduction test. The combined uncertainty for each test was averaged to obtain a final uncertainty for the calibration of  $3 \mu\text{V}/(\text{W}/\text{cm}^2)$ .

**Table C.1.** Uncertainty budget for the conduction calibration.

Source of Uncertainty	Standard Uncertainty
Measurement in $q''$ :	
Calibration of HFM	5% of measured $q''$
DAQ Uncertainty	3 $\mu\text{V}$
Measurement of $V$ :	
DAQ Uncertainty	3 $\mu\text{V}$

## Convection Calibration Uncertainty

The uncertainty for the convection calibration was estimated like the conduction calibration. First, the equation that was used to calculate the sensitivity of the HFA in the convection calibration

$$S_{HFA} = \frac{V_{HFA}}{h(\Delta T)} \quad (C.4)$$

which is used to determine the total uncertainty in the sensitivity measurement through the propagation of errors

$$\frac{u_c}{S_{HFA}} = \sqrt{\left(\frac{1}{V_{HFA}}\right)^2 u_{V_{HFA}}^2 + \left(\frac{1}{h}\right)^2 u_h^2 + \left(\frac{1}{\Delta T}\right)^2 u_{\Delta T}^2} \quad (C.5)$$

The uncertainty in the voltage measurement ( $u_v$ ) is the resolution of the DAQ which is 3  $\mu$ V. The uncertainty in the  $h$  measurement is the reported error for the HFM,  $\pm 5\%$  of the reading and the error in the thermocouple measurements which is 2.2  $^{\circ}$ C. The error in the  $h$  measurement was combined in the least squares sense to determine an  $u_h$  of 0.0612 W/(m-K). Finally, the uncertainty in the temperature measurement is the thermocouple error of 2.2  $^{\circ}$ C. Combining all of the uncertainties using Equation C.5 results in a combined uncertainty of 4  $\mu$ V/(W/cm<sup>2</sup>) using the uncertainty budget in Table C.2.

**Table C.2.** Uncertainty budget for the convection calibration.

Source of Uncertainty	Standard Uncertainty
Measurement of $h$ :	
Calibration of HFM	5% of measured $q''$
DAQ Uncertainty	3 $\mu$ V
Thermocouple Uncertainty	2.2 $^{\circ}$ C
Measurement of $V$ :	
DAQ Uncertainty	3 $\mu$ V
Measurement of $T$ :	
Thermocouple Uncertainty	2.2 $^{\circ}$ C

## Seebeck Coefficient Uncertainty

The uncertainty in the measurement of the Seebeck coefficient is estimated with the same procedure as the other calibrations. From Equation 1.4 the equation for the Seebeck coefficient is

$$Se = \frac{V_o}{\Delta T} \quad (C.6)$$

Propagation of error yields the equation for the combined uncertainty

$$\frac{u_c}{Se} = \sqrt{\left(\frac{1}{V}\right)^2 u_V^2 + \left(\frac{1}{T}\right)^2 u_T^2} \quad (C.7)$$

The uncertainty in the voltage measurement is the resolution of the multimeter, which is 5  $\mu$ V, and the uncertainty in the temperature measurement is the error for a type K

thermocouple of 2.2 °C. When Equation C.7 is combined with the measurements made in the Seebeck calibration an estimated uncertainty of 0.7  $\mu\text{V}/^\circ\text{C}$  is calculated using the uncertainty budget in Table C.3.

**Table C.3.** Uncertainty budget for the Seebeck coefficient calibration.

Source of Uncertainty	Standard Uncertainty
Measurement of V: Multimeter Uncertainty	5 $\mu\text{V}$
Measurement of T: Thermocouple Uncertainty	2.2 $^\circ\text{C}$

## Time Response Uncertainty

The time response was calculated by evaluation of voltage values that were measured by a DAQ. In order to do this, each voltage signal was investigated through the use of a MATLAB program. The program allowed the user to zoom in on the region of interest in the data, and determine when the voltage was not equal to an average zero value to determine a starting time ( $t_0$ ). Then, the time to reach 63% of the average full scale voltage output ( $t_{63\%}$ ) was found. These were subtracted to find the response time ( $t_r$ ), so the equation for the response of the HFA is

$$t_r = t_{63\%} - t_0 \quad (\text{C.8})$$

The deviation of both of the average values was calculated, and the 95% confidence interval for each of the measurements was used to establish the zero and full scale voltage values for the step input. Based upon Equation C.8, the propagation of error for the time response test is

$$\frac{u_c}{t_r} = \sqrt{u_{63\%}^2 + u_0^2} \quad (\text{C.9})$$

Since the  $t_{63\%}$  measurement is found by MATLAB, and the average zero and average full scale values are found to the 95% confidence interval,  $u_{63\%}$  is taken to be the resolution of the time measurements themselves and the uncertainty caused by the motion of the block that created the step. The time measurement uncertainty is equal to the sampling frequency of the DAQ which was 3000 Hz. The uncertainty caused by the movement of the block through the laser beam is estimated to be 2.5 ms. The two uncertainties are combined in a least squares sense to calculate a  $u_{63\%}$  of 2.5 ms.

The  $t_0$  measurement contains the same uncertainty in the sampling frequency as the  $t_{63\%}$  measurement, and also is subject to the program users' ability to select the correct starting point. Based on experience, the user can select the starting point within six data points, or 2 ms. The uncertainty for  $t_0$  is combined in the least squares sense, yielding  $u_0$ . Then, through the use of Equation C.9 the total uncertainty in time response experiment can be calculated to be 3.2 using the uncertainty budget found in Table C.4.

**Table C.4.** Uncertainty budget for the time response calibration.

Source of Uncertainty	Standard Uncertainty
Measurement of $t_{63\%}$ DAQ time resolution	0.3 ms
Measurement of $t_0$ : DAQ time resolution User selection of $t_0$	0.3 ms 2 ms
Creation of step input: Movement of metal block	2.5 ms

## Appendix D: Additional Experimental Results

In an attempt to obtain better results in the conduction calibration, additional data was taken. Measures were taken to improve the quality of the experiment. The main contributor to increased continuity was the use of a heated thumb to apply the heat flux. A Ziploc bag was heated with hot water, and Dave Hubble's thumb was heated using the water in the bag. Then, Dave pressed his thumb onto the HFA, applying enough pressure to minimize the contact resistance between the HFA and HFM. Different approaches were taken including using the hot water bag as the heat flux source and applying oil between the HFM and HFA to minimize the contact resistance. Neither of these techniques provided the consistent heat flux that Dave was able to achieve with his thumb.

The conduction test was performed on two different junctions of the HFA. Five different calibrations were performed with the heat flux going in each direction (side one and side two) with the results plotted in Figure D.1. In order to confirm that the tests from junction two-side two (plotted as junction 2-1, sides 1 and 2) were not a flipped version of junction one-side two, junction two was retested with the polarity of the gage switched in the DAQ and is reported as junction 2-2, sides 1 and 2. Similar results to the first test of junction two were obtained indicating that the differences in junctions one and two are physical differences that are not dependent on the way that the gage is hooked to the measurement device. The sensitivities recorded in this additional calibration average to  $25.2 \pm 1 \mu\text{V}/(\text{W}/\text{cm}^2)$ , where the uncertainty is calculated using the techniques presented in Appendix C. The 95% confidence interval for the data collected is  $11 \mu\text{V}/(\text{W}/\text{cm}^2)$ , an improvement from the data discussed from the conduction calibration section of the thesis. The spread in the data indicates that there is some variation from junction to junction. However, a new gage needs to be constructed with ten working junctions before this can be verified.

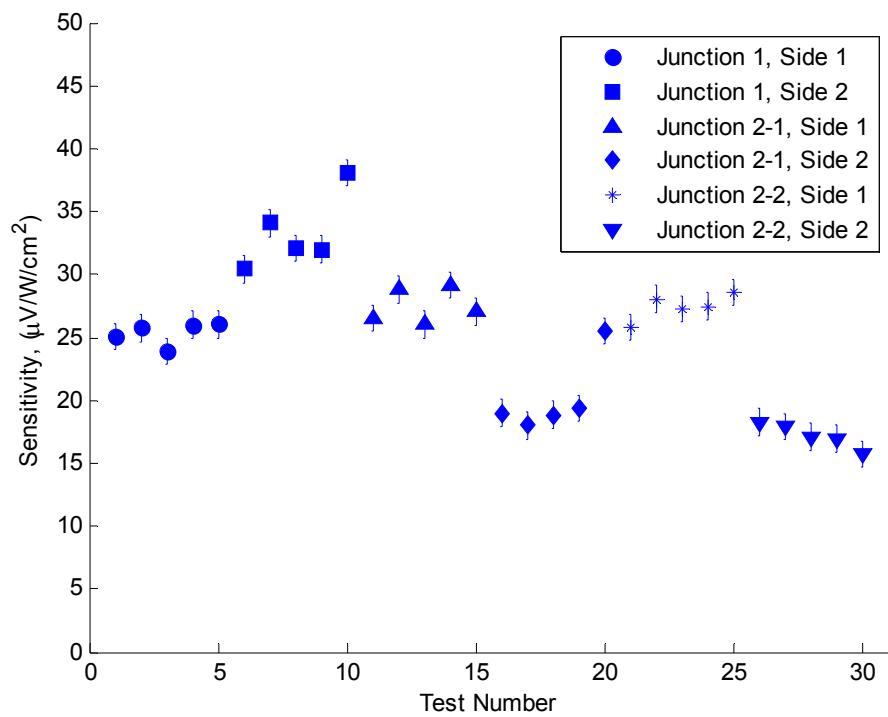


**Figure D.1.** Additional conduction calibration results.